Cesium-Anchored MB_3 Kagome Monolayers: Stabilizing Active Sites for Bifunctional Oxygen Electrocatalysis

Yaowen Long and Hong Zhang*
College of Physics, Sichuan University, 610065 Chengdu, China
Corresponding author: Hong Zhang, E-mail: hongzhang@scu.edu.cn

Table S1. Formation Energy E_{form} (eV) of $TM@BeB_3$, $TM@CaB_3$ and $TM@SrB_3$.

$TM@BeB_3$	E_{form}	$TM@CaB_3$	E_{form}	$TM@SrB_3$	E_{form}
Co	1.75	Co	-1.13	Co	-1.59
Cr	2.41	Cr	-0.92	Cr	-1.00
Cu	1.83	Cu	-0.10	Cu	-0.50
Fe	2.06	Fe	-0.98	Fe	-1.43
Mn	2.28	Mn	-0.90	Mn	-1.33
Ni	1.20	Ni	-0.92	Ni	-1.36
Ti	2.06	Ti	-1.98	Ti	-2.26
V	2.78	V	-1.25	V	-1.50

Table S2. Adsorption free energies (eV) and overpotentials (V) of the intermediate states of MB_3 in the OER and ORR processes.

Structure	ΔG_{OH*}	ΔG_{O*}	ΔG_{OOH*}	η_{OER}	η_{ORR}
$Co@BeB_3$	-0.57	0.53	2.57	1.12	1.80
$Cr@BeB_3$	-1.38	-1.12	1.96	1.90	2.61
$Cu@BeB_3$	-0.57	1.64	2.80	0.98	1.80
$Fe@BeB_3$	-0.76	-0.02	2.40	1.29	1.99
$Mn@BeB_3$	-1.30	-0.8	1.99	1.70	2.53
$Ni@BeB_3$	-0.18	1.46	3.06	0.63	1.41
$Ti@BeB_3$	-1.52	-0.34	1.94	1.75	2.75
$V@BeB_3$	-2.25	-2.04	1.33	2.36	3.48
$Co@CaB_3$	0.41	1.43	3.47	0.81	0.82
$Cr@CaB_3$	-1.40	-1.08	1.96	1.81	2.63
$Cu@CaB_3$	0.67	2.72	3.85	0.82	0.56
$Fe@CaB_3$	-0.12	0.26	2.95	1.46	1.35
$Mn@CaB_3$	-0.91	-0.80	2.46	2.04	2.14
$Ni@CaB_3$	0.82	2.33	3.93	0.37	0.41
$Ti@CaB_3$	-1.48	-0.40	1.78	1.91	2.71
$V@CaB_3$	-1.72	-0.98	1.61	2.08	2.95
$Co@SrB_3$	0.49	1.59	3.59	0.77	0.74
$Cr@SrB_3$	-1.54	-1.27	1.78	1.91	2.77
$Cu@SrB_3$	0.85	2.98	3.93	0.90	0.38
$Fe@SrB_3$	-0.05	0.33	3.01	1.45	1.28
$Mn@SrB_3$	-0.85	-0.70	2.54	2.01	2.08
$Ni@SrB_3$	0.92	2.77	2.98	0.71	1.02

$Ti@SrB_3$	-1.45	-0.33	1.82	1.87	2.68
$V@SrB_3$	-1.73	-0.99	1.61	2.09	2.96

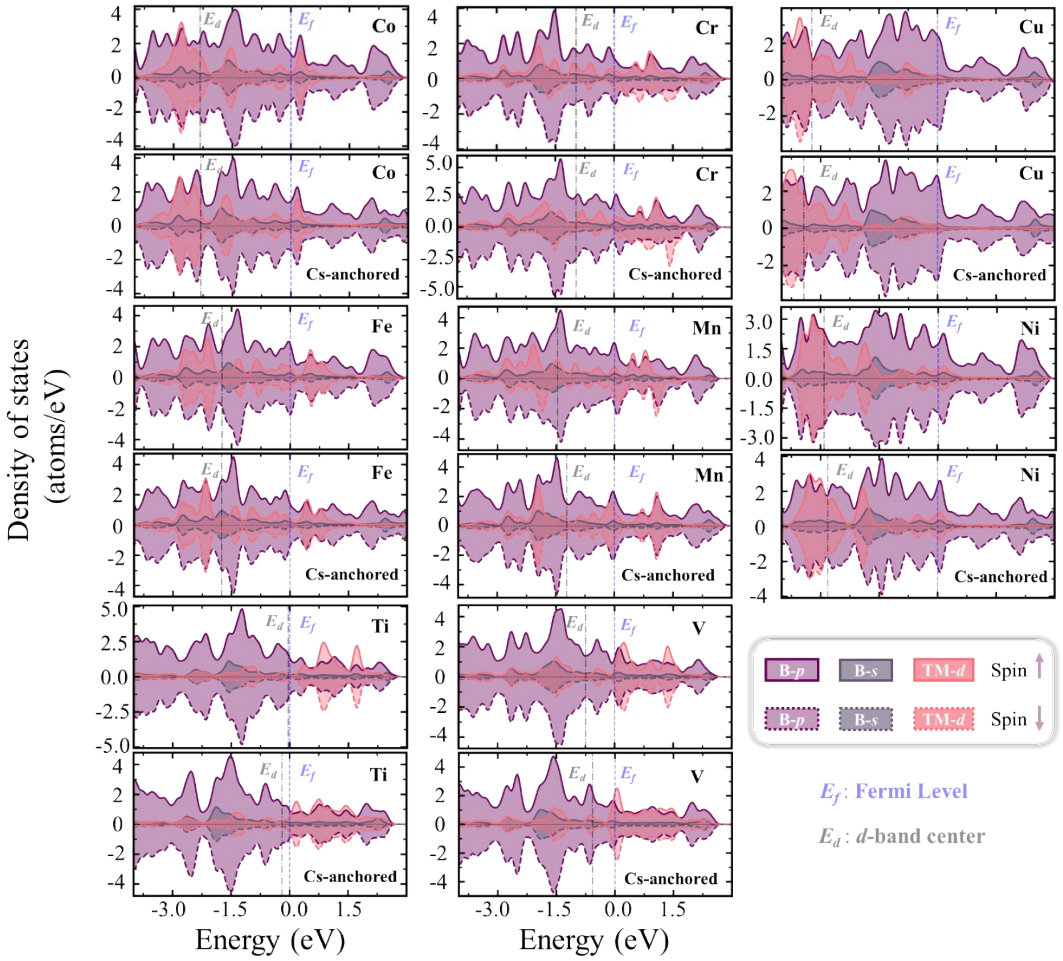

Figure S1. Projected density of states (PDOS) of $TM@CaB_3$ with/without Cs-anchored. The fermi-level and *d*-band center are indicated with dash vertical lines.

Table S3. The charge transfer of $TM@CaB_3$ and Cs-anchored $TM@CaB_3$ in the HER process via Bader charge analysis.

$TM@CaB_3$	$TM@CaB_3$		Cs-anchored		
	TM	H	TM	H	Cs
Co	-0.06	0.34	-0.11	0.44	-0.72
Cr	-0.80	0.43	-0.59	0.56	-0.73
Cu	-0.51	0.40	-0.52	0.60	-0.76
Fe	-0.30	0.31	-0.46	0.47	-0.73
Mn	-0.24	0.32	-0.26	0.47	-0.73
Ni	0.30	0.30	-0.01	0.48	-0.77
Ti	-1.28	0.61	-1.27	0.71	-0.78
V	-0.97	0.53	-1.03	0.63	-0.74

Table S4. The TM-Boron bond length ℓ_{bond} (Å) of $TM@BeB_3$, $TM@CaB_3$ and $TM@SrB_3$.

$TM@BeB_3$	ℓ_{bond}	$TM@CaB_3$	ℓ_{bond}	$TM@SrB_3$	ℓ_{bond}
Ti-B	2.32	Ti-B	2.18	Ti-B	2.19
V-B	2.16	V-B	2.09	V-B	2.10
Cr-B	2.38	Cr-B	2.05	Cr-B	2.05
Mn-B	2.12	Mn-B	1.99	Mn-B	2.00
Fe-B	2.12	Fe-B	1.97	Fe-B	1.98
Co-B	2.12	Co-B	1.95	Co-B	1.96
Ni-B	2.14	Ni-B	1.94	Ni-B	1.95
Cu-B	2.27	Cu-B	2.07	Cu-B	1.99

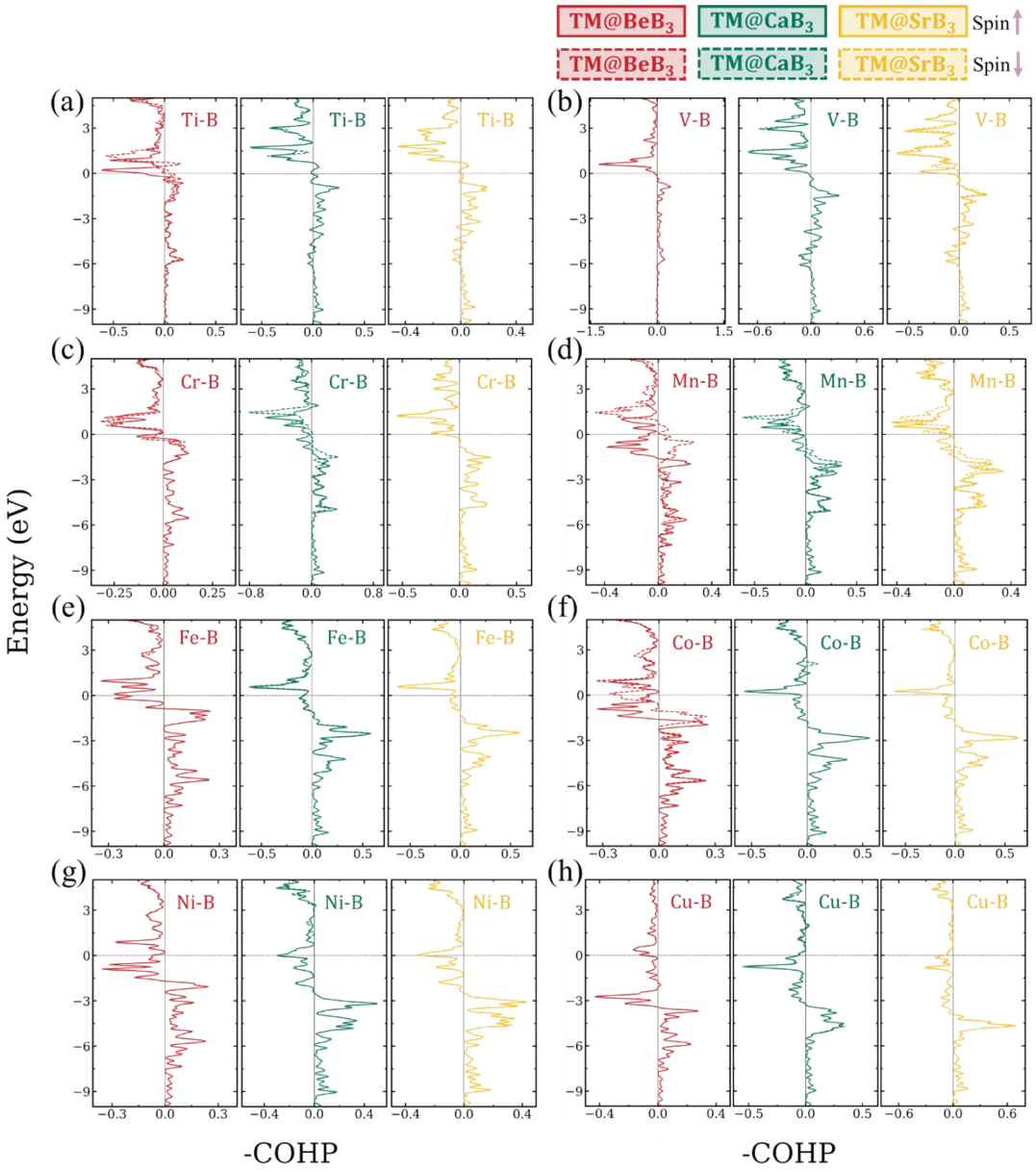

Figure S2. Projected Crystal Orbital Hamiltonian Population (pCOHP) analysis of TM–B bonds in $TM@BeB_3$, $TM@CaB_3$, and $TM@SrB_3$ across various spin states.

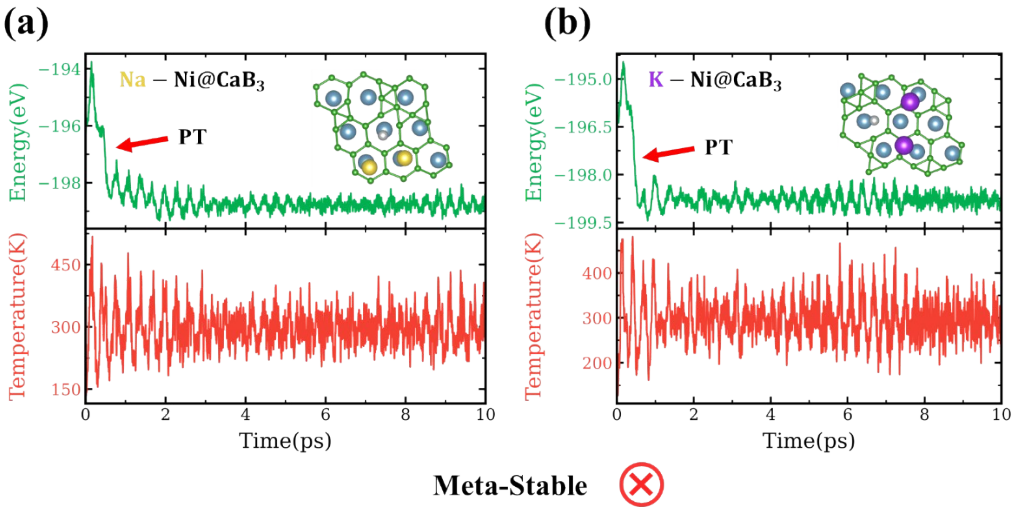

Figure S3. Structural evolution of (a) Na-anchored Ni@MB₃ and (b) K-anchored Ni@MB₃ at 300 K.

Table S5. Comparison of adsorption free energies (eV) and OER overpotentials (V) for intermediate states on BeB₃ with and without spin-orbit coupling (SOC)

	OER-noSOC	OER-SOC
ΔG_{OH*}	-0.465	-0.466
ΔG_{O*}	0.242	0.242
ΔG_{OOH*}	2.854	2.853
η_{OER}	1.382	1.381

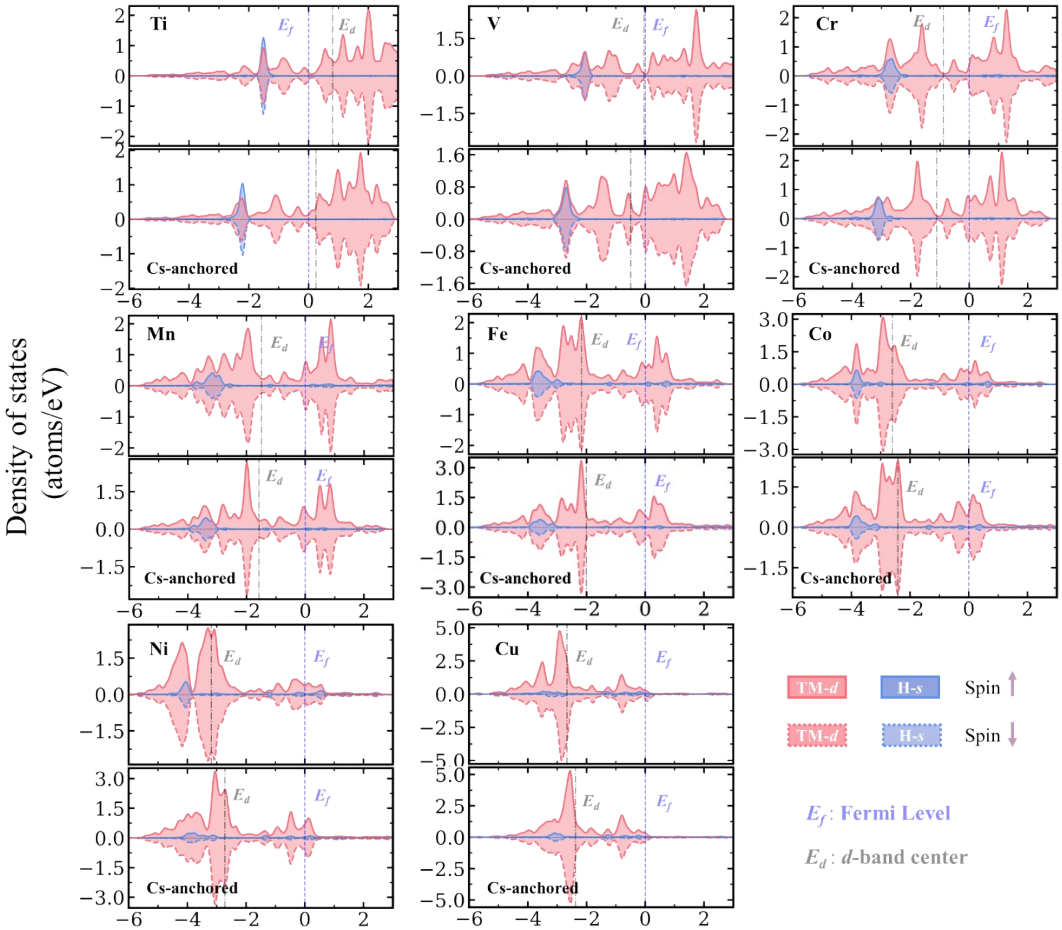

Figure S4. Projected density of states (PDOS) for TM@CaB_3 under the condition of hydrogen adsorption, with and without Cs anchoring. The Fermi level and d-band center are marked by vertical dashed lines.

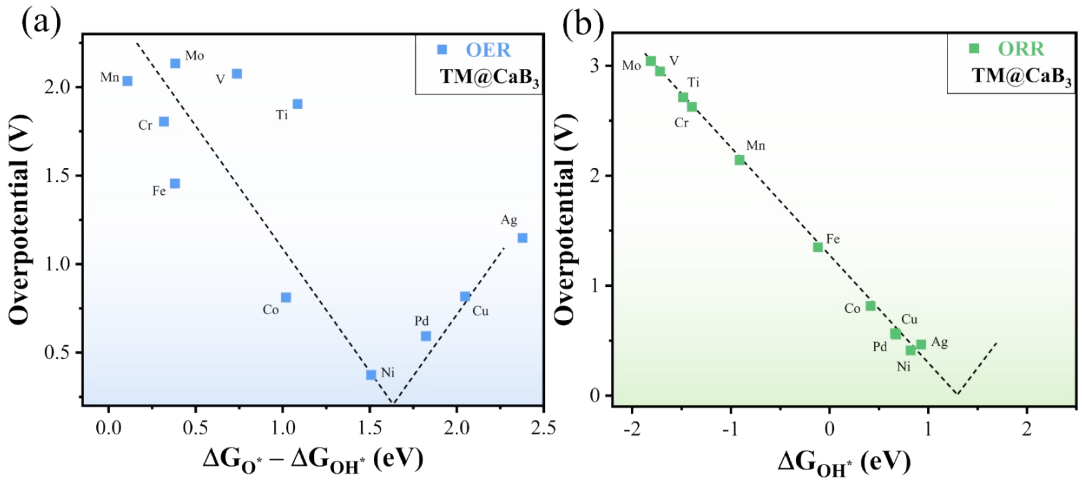

Figure S5. Volcano relationships for TM@CaB_3 (including additional Ag, Pd, Mo) (a) OER overpotential versus $\Delta G_{O*} - \Delta G_{OH*}$, (b) ORR overpotential versus ΔG_{OH*}.